Large-Scale Noniridescent Structural Color Printing Enabled by Infiltration-Driven Nonequilibrium Colloidal Assembly

*Ling Bai, Van Cuong Mai, Yun Lim, Shuai Hou, Helmuth Möhwald, and Hongwei Duan**

Structural colors originating from interaction of light with intricately arranged micro-/nanostructures have stimulated considerable interest because of their inherent photostability and energy efficiency. In particular, noniridescent structural color with wide viewing angle has been receiving increasing attention recently. However, no method is yet available for rapid and large-scale fabrication of full-spectrum structural color patterns with wide viewing angles. Here, infiltration-driven nonequilibrium assembly of colloidal particles on liquid-permeable and particle-excluding substrates is demonstrated to direct the particles to form amorphous colloidal arrays (ACAs) within milliseconds. The infiltration-assisted (IFAST) colloidal assembly opens new possibilities for rapid manufacture of noniridescent structural colors of ACAs and straightforward structural color mixing. Full-spectrum noniridescent structural colors are successfully produced by mixing primary structural colors of red, blue, and yellow using a commercial office inkjet printer. Rapid fabrication of large-scale structural color patterns with sophisticated color combination/layout by IFAST printing is realized. The IFAST technology is versatile for developing structural color patterns with wide viewing angles, as colloidal particles, inks, and substrates are flexibly designable for diverse applications.

A diverse range of natural creatures have evolved to generate distinct colors based on photonic micro-/nanostructures.[1] These so-called structural colors are photostable, energy efficient,[2] and often iridescent, therefore stimulating widespread interest in applications ranging from backlight-free displays[3] and anticounterfeiting techniques[4] to colorimetric sensors,[5] lasing[6] and solar cells.[7] Exploiting colloidal assembly[8] to prepare colloidal arrays is the most commonly used approach to developing structural colors. Colloidal crystals (CCs), as the most widely investigated photonic materials, are usually fabricated by evaporation,[9] internal[10] or external potentials/force[11,16]-driven colloidal crystallization. The spatially ordered structures of CCs give rise to a photonic band gap, which leads to vivid, metallic structural colors, and also to a variety of exciting fundamental effects (i.e., slow light effects[12] and spontaneous emission control[13]). On the other hand, the iridescent color of CCs caused by Bragg diffraction becomes a major problem in developing structural color-based sensors or displays, in which wide viewing angles are necessary. As such, amorphous colloidal arrays (ACAs) with noniridescent structural colors have attracted increasing attention. In the short-range ordered ACAs,[14] constructive interference of multiple scattering[15] yields noniridescent structural colors, whereas angle-dependent Bragg diffraction of light is greatly suppressed. Different from CCs, the key to fabricate ACAs is to avoid colloidal crystallization. ACAs have been prepared by taking advantage of bidisperse suspensions,[16] high viscosity media,[17] soft particles,[18] rapid evaporation,[19] or flocculation[20] for colloidal assembly. Notably, ACAs tend to display a pale color with increasing thicknesses due to strong multiple scattering light, which significantly affects the quality of their colors. To address this problem, black substances like carbon black[19a,c] or black background[20b] were used to absorb multiple scattered light, and successfully improved the quality of their structural colors.

Despite recent progress in preparing tailored colloidal arrays, rapid and large-scale structural color printing remains technically challenging. The primary bottleneck lies in the difficulty in rapid formation of colloidal arrays without reducing the quality of the structural colors. As the size of colloidal particles and the assembly conditions need to be tailored to produce different colors, it is exceedingly difficult for existing approaches to achieve high-speed fabrication of full-spectrum structural color patterns. In particular, the strong tendency of colloidal particles to crystallize makes it even more challenging to develop multicolored ACA patterns with wide viewing angles.

Herein, we develop a new method for rapid fabrication of noniridescent structural colors by nonequilibrium assembly of ACAs on permeable substrates driven by liquid infiltration. Theoretical analysis and experiments were first performed on a well-defined substrate, i.e., anodic aluminum oxide (AAO) membrane. The rapid infiltration in the AAO membrane causes

Dr. L. Bai, V. C. Mai, Y. Lim, Dr. S. Hou, Prof. H. W. Duan
School of Chemical and Biomedical Engineering
Nanyang Technological University
70 Nanyang Drive, Singapore 637457, Singapore
E-mail: hduan@ntu.edu.sg
V. C. Mai
Nanyang Environment and Water Research Institute (NEWRI)
Nanyang Technological University
1 Cleantech Loop, Singapore 637141, Singapore
Prof. H. Möhwald
Max Planck Institute of Colloids and Interfaces
14476 Potsdam, Germany
The ORCID identification number(s) for the author(s) of this article can be found under https://doi.org/10.1002/adma.201705667.

DOI: 10.1002/adma.201705667

© 2018 WILEY-VCH Verlag GmbH & Co. KGaA, Weinheim

a downward microflow in the colloidal dispersion, which transports the particles down and subsequently fixes them on the substrates. As colloidal crystallization is greatly suppressed in this nonequilibrium state,[21] ACAs are finally formed within milliseconds. In contrast, if the colloidal inks are not fully removed by infiltration on the substrates, the structures formed can be tailored from ACAs to CCs, when more liquid is left for evaporation. Colloidal assembly on flexible photo papers was further investigated. In the presence of downward infiltration flow, ACAs with vivid noniridescent colors were successfully prepared. A full-spectrum structural color CIE chromaticity diagram was achieved by the combination of red, blue, and yellow primary structural colors in real time. Large-scale landscape paintings with sophisticated combination and arrangement of colors were also demonstrated using a home printer at a speed higher than 10 cm^2 s^{-1}. With readily tailored colloidal particles, inks and substrates, our infiltration-assisted (IFAST) structural color printing method is a versatile technology for large-scale manufacture of structural color patterns, which is of great importance for the development of flexible sensors/solar cells and full-color paper-like displays.

AAO membranes with uniform, size-controlled cylindrical pores penetrating the entire membrane are ideal substrates for quantitative analysis of liquid infiltration. Water droplets of 300 pL in volume were printed onto an AAO membrane with 90 nm pores (Figure S1, Supporting Information). The entire shape of a droplet falling onto an AAO substrate (**Figure 1**a) was captured by a high-speed camera. The droplet volume quickly decreased and vanished within 0.9 ms, caused by strong downward infiltration. Colloidal assembly on an AAO membrane was subsequently investigated. Polystyrene (PS) (230 nm) colloidal droplets of the same volume were printed on the same AAO membrane. The colloidal droplets were dried immediately, leaving self-assembled PS particles in an amorphous arrangement, as displayed in Figure 1b. The degree of order of the colloidal arrays was examined by 2D fast Fourier transform (2D-FFT) analysis. Figure S2a in the Supporting Information shows a 2D-FFT pattern with bright concentric circles, indicating the existence of spatial correlation lengths between particles that is commonly found in a short-range ordered colloidal array. Specular reflection spectra of the colloidal arrays were also measured at incidence angles between 0° and 45° (see Figure S3a, Supporting Information). As shown in Figure 1c, the reflection peaks hardly move with increasing incidence angles, indicating a high degree of disorder.

Figure 1d presents the model, which we use for analyzing the infiltration-driven colloidal assembly on the AAO membrane, based on the following assumptions: (1) the contact line of the droplet is pinned during the whole solvent removal process; (2) the pores of the AAO membrane are smaller than the size of PS particles, and solvent infiltration is governed by the Washburn equation;[22] (3) the vertical speed of infiltration flow in the cylindrical pores and the vertical speed of microflows at the bottom of the droplet are independent of the radial distance to the drop center; and (4) the contact angles of the AAO membrane and its pores are independent of each other.

For an AAO membrane with a contact angle in its pores smaller than 90°, the instantaneous infiltration length[23] $L(t)$ in the AAO membrane at time t is given by

$$L(t) = \sqrt{\frac{\sigma d_{\text{pore}} t \cos\theta}{4\mu}} = kt^{\frac{1}{2}} \quad (1)$$

where θ is the intrinsic contact angle of the pore, d_{pore} is the average pore size of the AAO membranes, μ and σ are the dynamic viscosity and the surface tension, respectively, of the liquid (here water), and k is the capillary coefficient. The

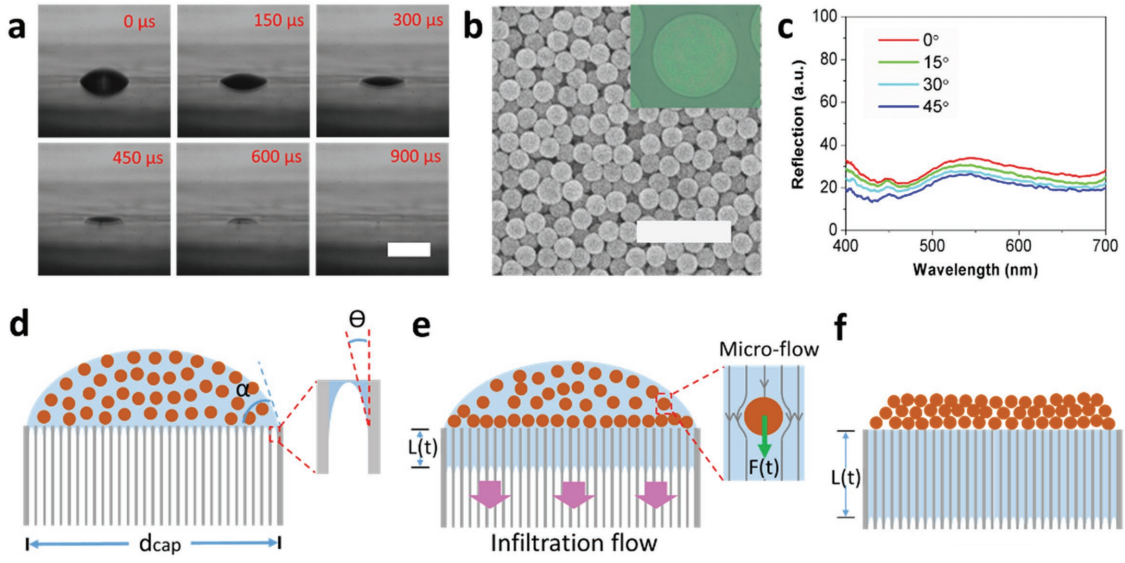

Figure 1. a) High-speed camera images of the entire process for water droplet removal on an AAO membrane, scale bar: 100 µm. b) SEM image of a colloidal array prepared on an AAO membrane, scale bar: 1 µm. The inset picture is the microscope image of printed single microdots with an integration time of 100 ms. c) Reflection spectra of ACAs at increasing incidence angles. d–f) Illustration of the formation of ACAs due to a strong downward infiltration flow.

© 2018 WILEY-VCH Verlag GmbH & Co. KGaA, Weinheim

instantaneous speed of the downward flow $V_D(t)$ in the droplet caused by infiltration is given by

$$V_D(t) = \varepsilon \frac{dL(t)}{dt} = \frac{\varepsilon k t^{-\frac{1}{2}}}{2} \quad (2)$$

where ε is the pore volume fraction of the AAO membrane. For a colloid particle with radius r that is held at a constant position, it experiences a downward Stokes drag[24] exerted by the downward flow

$$F(t) = 6\pi\mu r V_D(t) \quad (3)$$

This downward flow transports the colloidal particles toward the surface of the porous substrates. The Péclet number Pe here is set by the downward Stokes drag force to thermal forces

$$Pe = F(t)r/(k_b T) \quad (4)$$

where k_b is the Boltzmann constant and T is the temperature. For a spherical-capped droplet with volume V_{cap}, a drop deposition diameter d_{cap}, and an instantaneous contact angle α of the drop on the AAO membrane, the time for the AAO membrane to fully absorb the droplet equals[25]

$$t = \frac{\mu d_{cap}^2 \tan^2\frac{\alpha}{2}}{4\varepsilon^2 \sigma d_{pore} \cos\theta} \quad (5)$$

For an AAO membrane with thickness of 65 μm, d_{pore} = 90 nm, ε = 42.9%, α = 70°, if we assume θ to vary from 10° to 85°, it takes 0.35–4 ms to fully remove a 300 pL water droplet by infiltration, and the corresponding Péclet numbers at the end of infiltration vary from 804 to 21. It reveals that the Stokes drag force is too strong for diffusion to restore the equilibrium of colloidal particles in the suspension. The influence of Brownian motion caused by thermal energy is negligible compared with the downward microflow, which transports the particles to the substrate and traps them there. Since the particles in a certain volume of liquid removed by infiltration are fixed immediately on the substrates, the concentration of particles in the suspension remains nearly constant during colloidal assembly. As the driven force for colloidal crystallization is missing in this non-equilibrium state, a disordered packing of particles is finally formed.

For a better understanding of infiltration-driven colloidal assembly, we also investigated the situation where the colloidal ink was not fully removed by infiltration. The entire removal processes of a water drop on AAO membranes with a series of contact angles (Figure S4, Supporting Information) were investigated. As the contacting areas between the droplet and AAO membranes decreased at increasing contact angles, the maximum amount of water that can be removed by infiltration also decreased (Table S1, Supporting Information). When the contact angle was less than 40°, the droplet was fully removed by infiltration, the colloidal arrays were always composed of a disordered arrangement of particles, as shown in Figure S5a in the Supporting Information. However, with further increase of the contact angle from 60° to 95°, the droplet could not be fully removed by infiltration (see **Figure 2**a,b), as the AAO membranes were saturated. In both images, contact angles in cylindrical pores are smaller than 90°, as the droplet volume quickly decreased in the first 3–4 ms due to infiltration. After the infiltration ended, it took another 200–800 ms for evaporation of the remaining water depending on its volume. PS colloidal droplets of similar volumes were subsequently printed on AAO membranes with a contact angle of 60°, 75°, and 95°. The colloidal arrays printed on three AAO membranes all showed bright green color. With increase of contact angles, the arrangement of particles gradually shifted from partly ordered (Figure 2c), polycrystalline (Figure S5b, Supporting Information), to long-range ordered (Figure 2d; Figure S6, Supporting Information). Compared with that of ACAs, the 2D-FFT pattern of partly ordered colloidal arrays (PCAs) in Figure 2c displays bright concentric circles with a higher number of rings (Figure S2b, Supporting Information), indicating a higher degree of order. The 2D-FFT pattern of CCs in Figure 2d shows sharp hexagonal peaks (Figure S2c, Supporting Information), confirming the presence of long-range crystalline order. Specular reflection spectra of PCAs and CCs obtained on AAO membranes with a contact angle of 60° and 95° are also plotted in Figure 2e,f. In both cases, their reflection peaks blue-shift with increasing incidence angles. But the peak shift is much smaller for PCAs due to the disorder of PCAs, as light is not only specularly reflected, but also is scattered into other directions. In addition, the reflected intensity depends more on the incidence angle for the CCs, much less for the PCAs. These results also suggest that after infiltration stopped, the order of colloidal arrays could gradually evolve from amorphous to crystalline. We reason that once infiltration stopped, the particles were no longer fixed, and could be gradually transported back to suspension by Marangoni microflow[26] and Boltzmann motion. Because the subsequent self-assembly occurred in a near equilibrium state driven by entropy,[27] the degree of order of the colloidal arrays therefore significantly increased.

To manufacture structural color patterns, papers (Figure S7, Supporting Information) with strong solvent removing abilities (Figure S8, Supporting Information) are highly desirable as substrates. Previous studies[28] have investigated the infiltration in papers in details. Different from infiltration in AAO membranes, there is lateral infiltration in papers, as illustrated in **Figure 3**a. The lateral infiltration leads to a lateral microflow in the colloidal ink droplet, which transports the particles to the edge of the droplet, and finally leads to the formation of a coffee ring (Figure 3b). ACA microdots were first produced by printing 300 pL colloidal ink droplets onto black photo papers. The printed microdots (Figure 3c) are of well-ordered arrangement and all display vivid green structural color. The scanning electron microscopy (SEM) image of the cross-sectional view (Figure 3d) reveals the coffee-ring structure of the microdots, and the top-view SEM images show an amorphous arrangement of particles both in the center (Figure 3e) and at the edge (Figure S9, Supporting Information) of the microdot. These results suggest the successful fabrication of ACAs by IFAST printing and show the influence of lateral infiltration on colloidal assembly on paper.

© 2018 WILEY-VCH Verlag GmbH & Co. KGaA, Weinheim

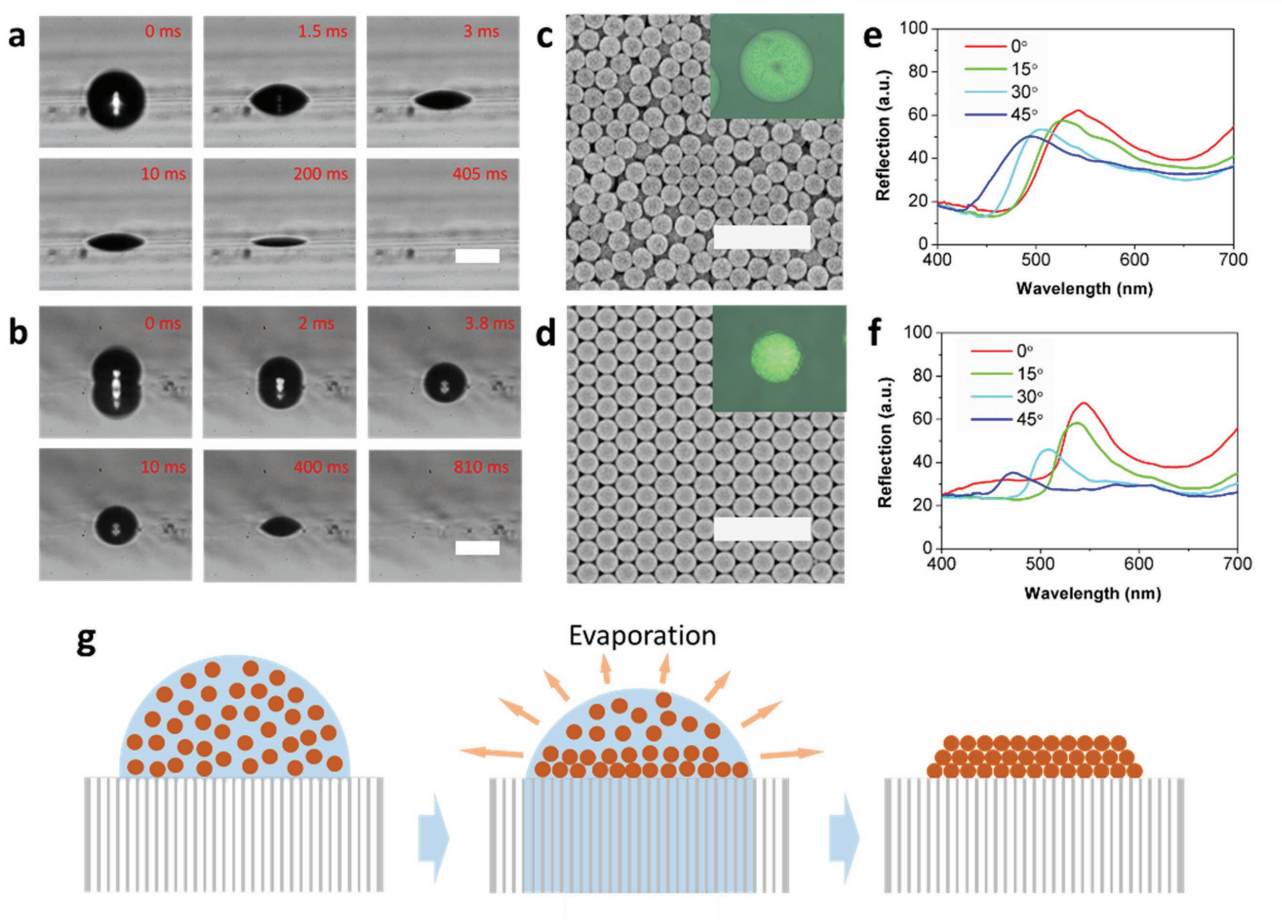

Figure 2. a,b) High-speed camera images of the entire process for water droplet removal on AAO membranes with a contact angle of 60° and 95°, scale bar: 100 µm. c,d) SEM images of colloidal array prepared on AAO membranes with a contact angle of 60° and 95°, scale bar: 1 µm. The inset pictures are the microscope images of printed single microdots with an integration time of 100 and 50 ms. e,f) Reflection spectra of corresponding ACAs at increasing incidence angles. g) Illustration of the changes of order range in the colloidal arrays driven by evaporation.

Structural color letters were subsequently printed to investigate their optical properties. Figure 3f displays the optical images of letters rotated at different angles under natural light. The color of letters hardly changed, when the angle of rotation was varied from 5° to 45°. The backscattering, specular reflection, and scattering spectra of the letters were subsequently measured, using the setup in Figure S3 in the Supporting Information. Backscattering spectra of the letters were first captured by fixing the detection arm while rotating the sample. The false color map (Figure 3g) shows the backscattering intensity of the letters as a function of the incidence angle and wavelength. When the angle of rotation increases from 10° to 15°, the peak intensity dramatically decreases, and peak wavelength is blue-shifted from 532 to 518 nm correspondingly. Afterward, the peak wavelength and intensity are nearly constant as the angle of rotation increases from 15° to 50°. These results suggest that the color of ACAs is almost noniridescent with the changes of rotation angles. The specular reflection and diffusive scattering spectra were subsequently measured, as shown in Figure 3h,i. The angle-dependent reflection peak shift of the ACAs is clearly observed when incident and viewing angles both change. Furthermore, the wavelength of scattering peaks blue-shifts from 534 to 512 nm when the view angle changes from 10° to 50°. Therefore the printed structural colors are iridescent with changes of incident and/-or viewing angles under direct illumination.

To achieve full-spectrum structural color printing, structural color mixing was explored. A home inkjet printer of CMYK color mode was used for the structural color mixing. SiO_2, PS, and core–shell polydopamine-coated PS particles (PS@PDA) with different surface charges and properties were explored for structural color printing (Figure S10, Supporting Information). PS@PDA particles were chosen because black substance such as PDA is able to suppress the multiple light scattering of ACAs, and thereby improves the quality of the structural colors printed. **Figure 4**a shows a structural color chart by secondary color mixing of three structural colors with certain increments of percent values. In the color mixing charts, the two primary colors are printed along two orthogonal axes on the top and the left-most lanes, respectively, with the saturation of structural colors increasing in equal percentage. Secondary colors are mixtures of the two orthogonal primary colors, and thus the hues of structural colors can also be tailored by percent values. A CIE chromaticity diagram was subsequently prepared using red–yellow–blue structural colors

© 2018 WILEY-VCH Verlag GmbH & Co. KGaA, Weinheim

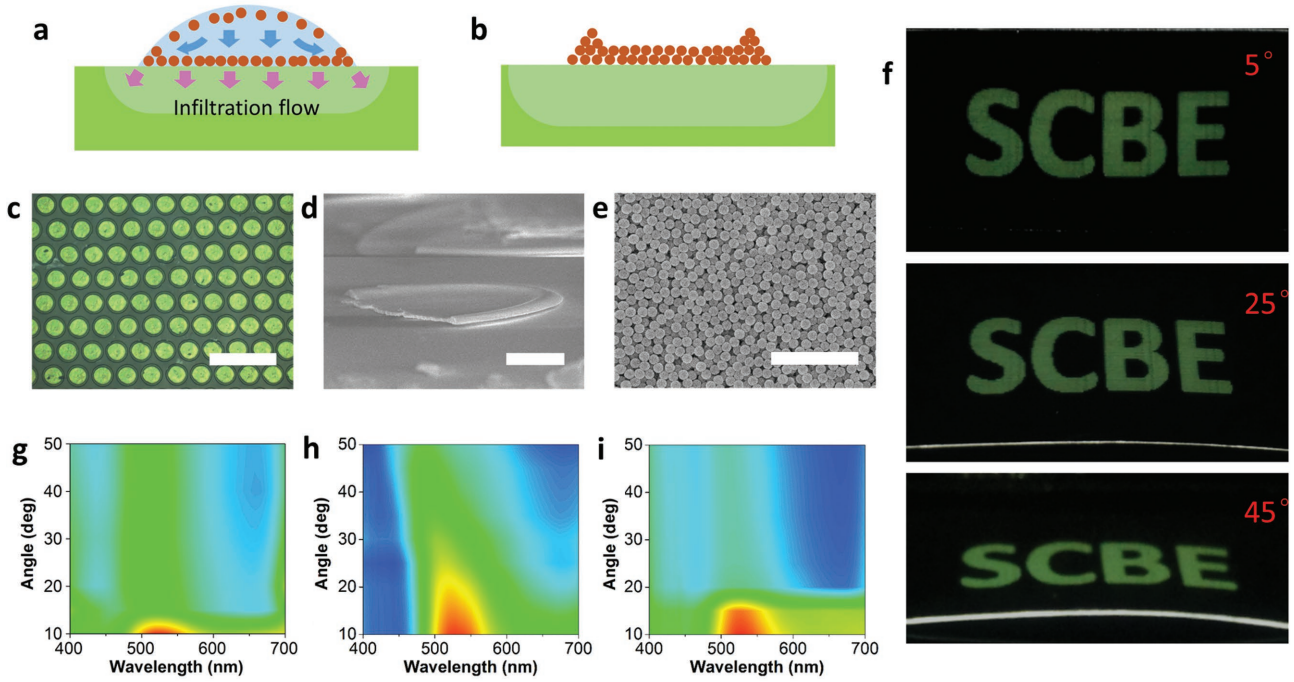

Figure 3. a) Illustration of the infiltration flow in papers and microflow inside a colloidal droplet. b) Illustration of self-assembled ACAs. c) Microscope image of the printed ACA dots, scale bar: 400 µm. d) Cross side-view SEM image of single ACA dot, scale bar: 30 µm. e) Top side-view SEM image of single ACA dot, scale bar: 2 µm. f) Photographs of inkjet printing SCBE letters at different rotation angles. g–i) False color maps showing the backscattering, reflection, and scattering intensity, respectively, as a function of the rotation/incidence angle and wavelength. Red and blue colors represent high and low intensities, respectively.

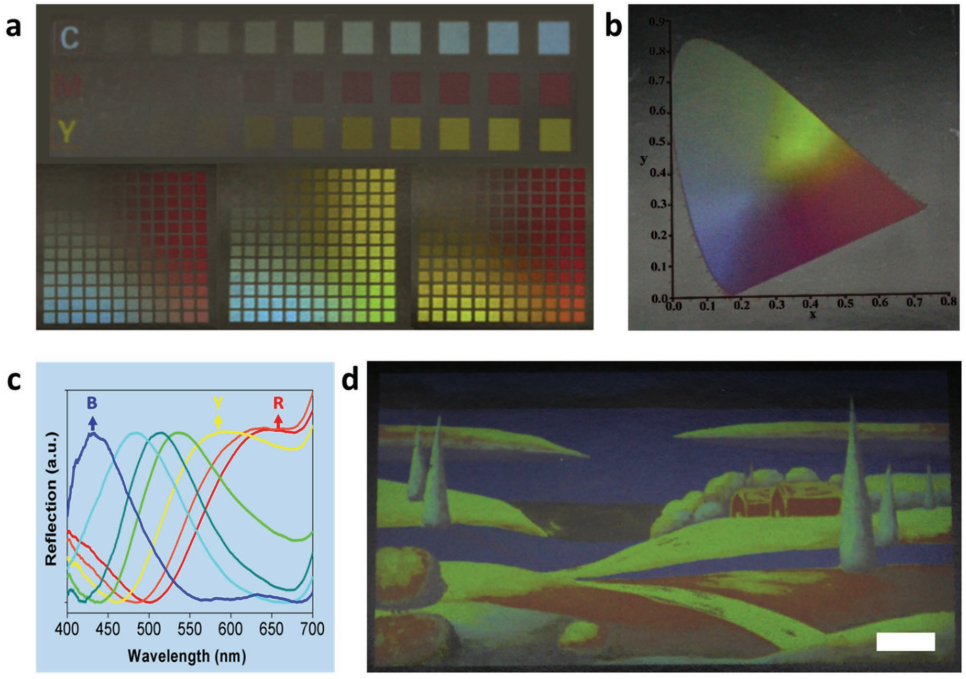

Figure 4. a) Printed primary and secondary mixed color chart made of cyan–yellow–red structural colors. b) A CIE chromaticity diagram obtained by color mixing of red–yellow–blue structural colors. c) Normalized reflection spectra of primary and secondary mixed structural colors in the color chart. d) A multicolored painting of a landscape with high resolution, scale bar: 1 cm.

© 2018 WILEY-VCH Verlag GmbH & Co. KGaA, Weinheim

to explore the achievable color gamut, as shown in Figure 4b. By changing the CMYK percent values, structural colors covering the full spectrum were obtained. The reflection peaks of mixed colors (Figure 4c) are between those of primary structural colors, different from the traditional subtractive CMYK color model. These results provide guidance to design full-spectrum structural color patterns. Large-scale full-spectrum structural color printing with high resolution was further demonstrated. Paintings of landscape with sophisticated color combination and layout (Figure 4d) were readily prepared using a home printer at a speed above 10 cm^2 s^{-1}. Structural colors with different hues, brightness, and saturation are included in the painting, and color transitions between neighboring parts of the picture are very smooth. All the patterns are composed of ACAs (Figure S11, Supporting Information) and display an almost isotropic color under natural light but iridescent colors with changing direct illumination/viewing angles (Figure S12, Supporting Information), and their colors are stable even after being bended repeatedly (Figure S13, Supporting Information). These results demonstrate an extremely simple and convenient way for general-purpose structural color printing with wide viewing angles and also hold great potential for the design of flexible structural color devices. The general applicability of this method has also been demonstrated by successful fabrication of ACAs on porous polymer substrates, such as polyamide and polyethersulfone membranes, as shown in Figure S14 in the Supporting Information.

In summary, we have developed a universal and versatile method for rapid fabrication of ACAs through infiltration-driven colloidal assembly on liquid-permeable substrates. The flowing colloidal suspensions directed by strong infiltration are far from equilibrium, suppressing colloidal crystallization but favoring the formation of ACAs. Rapid, scalable, high-resolution, and full-spectrum structural color patterns on liquid permeable substrates are achieved by IFAST printing, offering unprecedented flexibility in fabricating structural color patterns. A variety of colloidal particles and inks can be used for further development of structural color devices with tailored optical properties and functionalities. The substrates for IFAST printing are not limited to AAO membranes or photo papers, any substrates that are liquid-permeable but particle-impermeable are in principle suitable for our strategy. This method is of great potential for fabricating flexible sensors and full-color paper-like displays. By controlling liquid infiltration in the substrates, it is possible to develop sophisticated photonic structures with tailored spatial order or disorder, which is also important for fundamental study of Anderson localization or coherent backscattering of lights as well as applications of random lasers or solar cells.

Experimental Section

Capture of Water Droplets Infiltration on AAO Membranes: An inkjet printer head (MD-K-130, Microdrop, Germany) with an orifice diameter of 70 µm was used for generation of water droplets, controlled by a waveform generator (MD-E-201H, Microdrop, Germany). A high-speed camera (FastCam SA5 monochrome, Photron) was used to obtain images at 20 000 fps with a resolution of 704 × 520 pixels, under direct illumination by an ultrahigh pressure mercury lamp (Intensilight 130 W, Nikon). An X-Y stage (06DTS-1M, Unice) was used to accurately move the AAO membranes to the desired place.

Preparation of Latex Inks: PS and SiO_2 particles were acquired from Nanjing Nanorainbow Bio-technology Co., LTD. For the synthesis of PS@PDA, 200 mg PS particles and 100 mg dopamine were mixed with 200 mL Tris buffer (10×10^{-3} M, pH 8.5) under stirring overnight. The obtained PS@PDA particles were purified three times and redispersed in water for further usage. Printing inks were prepared by mixing 0.5 mL ethylene glycol with a latex suspension (2 mL) containing 7 wt% PS, SiO_2, or PS@PDA particles. All latex suspensions were placed in an ultrasonic bath for 10 min and filtered through micropore filters with a pore size of 0.5 µm before use.

IFAST Printing of Structural Color Patterns: Monocolor ACA patterns were obtained by IFAST printing on photo papers using a Jetlab 4 tabletop printing platform. Multicolored patterns were obtained using an M-10 Epson inkjet printer. Colloidal inks of SiO_2, PS, or PS@PDA particles were filled into cyan–yellow–magenta cartridges for printing. SiO_2 particles with an average particle size of 210 and 240 nm were used to create blue and cyan colors. PS particles with a diameter of 240 nm were used for printing yellow colors, and PS@PDA-1 with a size of 270 nm was used for printing red colors.

Characterization: Optical graphs were captured by a digital camera (EOS 700D, Canon). Micrographs were acquired by a CCD camera (CoolSnap, Photometrics), which was directly aligned to the inverted microscope (IX71, Olympus). SEM observations of arrangement of particles were conducted on a field emission scanning electron microscope (JSM-6700F, Japan). Transmission electron microscopy (TEM) images of particles were acquired on a Jeol JEM2010 electron microscope at an acceleration voltage of 300 kV. The 2D Fourier power spectra of the SEM images were obtained by using Matlab. Reflective, backscattering, and scattering spectra were recorded using a fiber optic UV–vis spectrometer (Ocean Optic HR2000CG). Contact angles were measured using a FTA200 contact angle analyzer.

Supporting Information

Supporting Information is available from the Wiley Online Library or from the author.

Acknowledgements

This work was supported by the Ministry of Education-Singapore (MOE2015-T2-1-112 and MOE2013-T3-1-002, and RG49/16).

Conflict of Interest

The authors declare no conflict of interest.

Keywords

amorphous colloidal array, infiltration, inkjet printing, nonequilibrium assembly, structural color printing

Received: September 29, 2017
Revised: November 26, 2017
Published online:

[1] A. G. Dumanli, T. Savin, *Chem. Soc. Rev.* **2016**, *45*, 6698.
[2] S. Kinoshita, S. Yoshioka, J. Miyazaki, *Rep. Prog. Phys.* **2008**, *71*, 076401.

© 2018 WILEY-VCH Verlag GmbH & Co. KGaA, Weinheim

[3] a) H. S. Kang, J. Lee, S. M. Cho, T. H. Park, M. J. Kim, C. Park, S. W. Lee, K. L. Kim, D. Y. Ryu, J. Huh, E. L. Thomas, C. Park, *Adv. Mater.* **2017**, *29*, 1700084; b) A. C. Arsenault, D. P. Puzzo, I. Manners, G. A. Ozin, *Nat. Photonics* **2007**, *1*, 468; c) H. Kim, J. Ge, J. Kim, S.-e. Choi, H. Lee, H. Lee, W. Park, Y. Yin, S. Kwon, *Nat. Photonics* **2009**, *3*, 534; d) M. Kuang, J. Wang, B. Bao, F. Li, L. Wang, L. Jiang, Y. Song, *Adv. Opt. Mater.* **2014**, *2*, 34; e) H. Gu, Y. Zhao, Y. Cheng, Z. Xie, F. Rong, J. Li, B. Wang, D. Fu, Z. Gu, *Small* **2013**, *9*, 2266; f) L. Tong, W. Qi, M. Wang, R. Huang, R. Su, Z. He, *Small* **2016**, *12*, 3433.

[4] L. Bai, Z. Xie, W. Wang, C. Yuan, Y. Zhao, Z. Mu, Q. Zhong, Z. Gu, *ACS Nano* **2014**, *8*, 11094.

[5] a) I. B. Burgess, M. Loncar, J. Aizenberg, *J. Mater. Chem. C* **2013**, *1*, 6075; b) C. Fenzl, T. Hirsch, O. S. Wolfbeis, *Angew. Chem., Int. Ed.* **2014**, *53*, 3318.

[6] S. Furumi, *J. Mater. Chem. C* **2013**, *1*, 6003.

[7] W. Zhang, M. Anaya, G. Lozano, M. E. Calvo, M. B. Johnston, H. Miguez, H. J. Snaith, *Nano Lett.* **2015**, *15*, 1698.

[8] a) G. von Freymann, V. Kitaev, B. V. Lotsch, G. A. Ozin, *Chem. Soc. Rev.* **2013**, *42*, 2528; b) S. Yoshioka, Y. Takeoka, *ChemPhysChem* **2014**, *15*, 2209.

[9] a) Z. Z. Gu, A. Fujishima, O. Sato, *Chem. Mater.* **2002**, *14*, 760; b) B. G. Prevo, O. D. Velev, *Langmuir* **2004**, *20*, 2099; c) J. Wang, L. Wang, Y. Song, L. Jiang, *J. Mater. Chem. C* **2013**, *1*, 6048; d) Y. Zhao, L. Shang, Y. Cheng, Z. Gu, *Acc. Chem. Res.* **2014**, *47*, 3632.

[10] J. H. Holtz, S. A. Asher, *Nature* **1997**, *389*, 829.

[11] a) P. V. Braun, R. W. Zehner, C. A. White, M. K. Weldon, C. Kloc, S. S. Patel, P. Wiltzius, *Adv. Mater.* **2001**, *13*, 721; b) J. Ge, Y. Hu, Y. Yin, *Angew. Chem., Int. Ed.* **2007**, *46*, 7428.

[12] J. Liu, H. Zhao, M. Wu, B. Van der Schueren, Y. Li, O. Deparis, J. Ye, G. A. Ozin, T. Hasan, B.-L. Su, *Adv. Mater.* **2017**, *17*, 1605349.

[13] A. C. Arsenault, T. J. Clark, G. von Freymann, L. Cademartiri, R. Sapienza, J. Bertolotti, E. Vekris, S. Wong, V. Kitaev, I. Manners, *Nat. Mater.* **2006**, *5*, 179.

[14] L. Shi, Y. F. Zhang, B. Q. Dong, T. R. Zhan, X. H. Liu, J. Zi, *Adv. Mater.* **2013**, *25*, 5314.

[15] a) R. O. Prum, R. H. Torres, S. Williamson, J. Dyck, *Nature* **1998**, *396*, 28; b) H. Noh, S. F. Liew, V. Saranathan, S. G. Mochrie, R. O. Prum, E. R. Dufresne, H. Cao, *Adv. Mater.* **2010**, *22*, 2871; c) Y. Takeoka, *J. Mater. Chem.* **2012**, *22*, 23299.

[16] a) Y. Takeoka, M. Honda, T. Seki, M. Ishii, H. Nakamura, *ACS Appl. Mater. Interfaces* **2009**, *1*, 982; b) J. D. Forster, H. Noh, S. F. Liew, V. Saranathan, C. F. Schreck, L. Yang, J. G. Park, R. O. Prum, S. G. Mochrie, C. S. O'Hern, *Adv. Mater.* **2010**, *22*, 2939.

[17] Q. Zhao, C. E. Finlayson, D. R. Snoswell, A. Haines, C. Schäfer, P. Spahn, G. P. Hellmann, A. V. Petukhov, L. Herrmann, P. Burdet, *Nat. Commun.* **2016**, *7*, 11661.

[18] J. G. Park, S. H. Kim, S. Magkiriadou, T. M. Choi, Y. S. Kim, V. N. Manoharan, *Angew. Chem., Int. Ed.* **2014**, *53*, 2899.

[19] a) Y. Takeoka, S. Yoshioka, A. Takano, S. Arai, K. Nueangnoraj, H. Nishihara, M. Teshima, Y. Ohtsuka, T. Seki, *Angew. Chem., Int. Ed.* **2013**, *52*, 7261; b) D. Ge, E. Lee, L. Yang, Y. Cho, M. Li, D. S. Gianola, S. Yang, *Adv. Mater.* **2015**, *15*, 2489; c) Y. Ohtsuka, T. Seki, Y. Takeoka, *Angew. Chem., Int. Ed.* **2013**, *127*, 15588.

[20] a) P. D. García, R. Sapienza, C. López, *Adv. Mater.* **2010**, *22*, 12; b) M. Iwata, M. Teshima, T. Seki, S. Yoshioka, Y. Takeoka, *Adv. Mater.* **2017**, *26*, 1605050.

[21] a) S. R. De Groot, P. Mazur, *Non-Equilibrium Thermodynamics*, Courier Corporation, USA **2013**; b) B. Wang, J. Kuo, S. C. Bae, S. Granick, *Nat. Mater.* **2012**, *11*, 481.

[22] E. W. Washburn, *Phys. Rev.* **1921**, *17*, 273.

[23] M. Denesuk, G. Smith, B. Zelinski, N. Kreidl, D. Uhlmann, *J. Colloid Interface Sci.* **1993**, *158*, 114.

[24] W. B. Russel, D. A. Saville, W. R. Schowalter, *Colloidal Dispersions*, Cambridge University Press, Cambridge, UK **1989**.

[25] M. Pack, H. Hu, D.-O. Kim, X. Yang, Y. Sun, *Langmuir* **2015**, *31*, 7953.

[26] H. Hu, R. G. Larson, *Langmuir* **2005**, *21*, 3972.

[27] V. J. Anderson, H. N. W. Lekkerkerker, *Science* **2002**, *416*, 811.

[28] a) V. Starov, S. Kostvintsev, V. Sobolev, M. Velarde, S. Zhdanov, *J. Colloid Interface Sci.* **2002**, *252*, 397; b) V. Starov, S. Zhdanov, M. Velarde, *Langmuir* **2002**, *18*, 9744.

© 2018 WILEY-VCH Verlag GmbH & Co. KGaA, Weinheim